Optimal Design of N-$\mathcal{UU}$ Parallel Mechanisms

Yuanqing Wu[1] and Marco Carricato[2]

[1]*Dept. of Industrial Engineering, University of Bologna, Italy, e-mail: yuanqing.wu@unibo.it*
[2]*Dept. of Industrial Engineering, University of Bologna, Italy, e-mail: marco.carricato@unibo.it*

Abstract. In this paper, we present the optimal design of N-$\mathcal{UU}$ ($\mathcal{U}$ stands for universal joints) parallel mechanisms (PM) with general geometry, for the achievement of maximal singularity-free tilt angle. We first briefly recall the synthesis condition and constraint analysis of the general N-$\mathcal{UU}$ PM, showing that static singularities may be factorized into active and passive constraint singularities. We then formulate the optimal design problem as the maximization of the end-effector tilt angle subject to closeness to active and passive constraint singularities. We conclude the paper by illustrating how an angle-equalizing device on the inner revolute pairs of the $\mathcal{UU}$ legs may help avoiding passive constraint singularities and increasing the maximal tilt angle.

Key words: symmetric subspace, parallel mechanism, singularity analysis, workspace optimization.

1 Introduction

It is well known that N-$\mathcal{UU}$ PMs are kinematically equivalent to a well known class of constant-velocity couplings with two rotational degrees of freedom (DoF) [8]. A special-geometry N-$\mathcal{UU}$ PM was first proposed in [6], followed by several rediscoveries of the same mechanism until recently [11, 12, 10]. Carricato [4] made a further clarification of the synthesis condition of the N-$\mathcal{UU}$ PM, which may be summarized as follows:

C1) The two $\mathcal{U}$ joints in each $\mathcal{UU}$ leg must be identical and remain in a mirror symmetric configuration during full-cycle motion; see Fig. 1(b).
C2) all $\mathcal{UU}$ legs share the same plane of symmetry and the revolute axes of the proximal (distal) $\mathcal{U}$ joints of all legs intersect at one point $\mathbf{s}^{+}$ ($\mathbf{s}^{-}$); see Fig. 1(c).

A comprehensive kinematic and singularity analysis of general-geometry N-$\mathcal{UU}$ PMs is conducted in [14]. In this paper, instead, we study the optimal design of these mechanisms for the maximization of the end-effector singularity-free tilt angle (simply referred to as tilt angle hereafter).

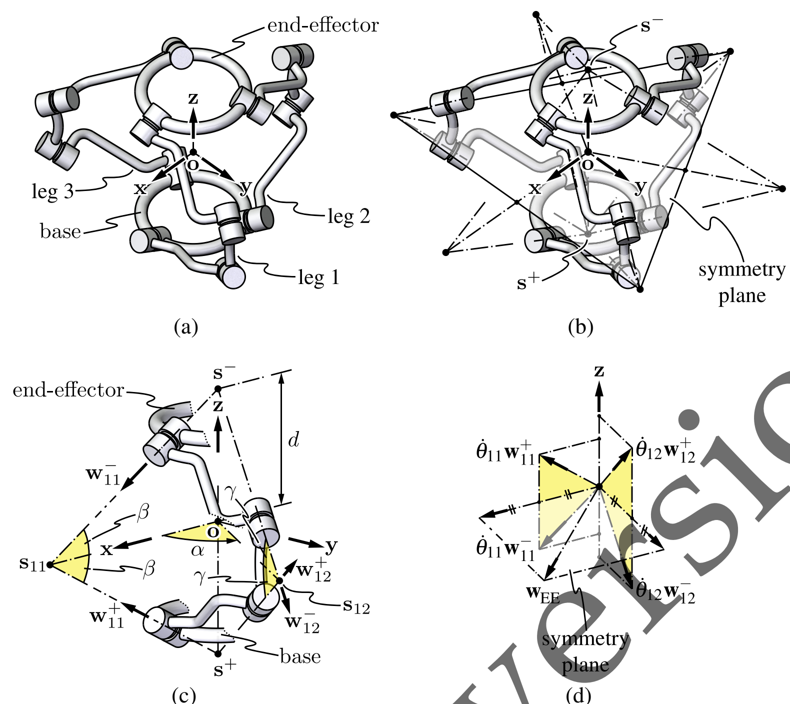

Fig. 1 Schematic of a general 3-$\mathcal{UU}$ PM: (a) components of the PM; (b) synthesis condition of the PM: the two $\mathcal{U}$ joints in each leg are mirror symmetric about the **xy**-plane, and the revolute axes of all proximal (or distal) $\mathcal{U}$ joints in all legs intersect at a point $\mathbf{s}^{+}$ (or $\mathbf{s}^{-}$); (c) geometry of the first leg; (d) end-effector angular velocity $\mathbf{w}_{\mathrm{EE}}$ under an instantaneous symmetric movement ($\dot{\theta}^{+}_{1j} = \dot{\theta}^{-}_{1j} = \dot{\theta}_{1j},\ j = 1,2$).

The paper is organized as follows. Section 2 recalls the most relevant results presented in [14]. We show that N-$\mathcal{UU}$ PMs may equivalently be studied as purely spherical mechanisms, so that their static singularities may be factorized into the degeneracy of a force bundle (active constraint singularity) and a torque bundle (passive constraint singularity). In Sec. 3, we propose two formulations for the optimal design of N-$\mathcal{UU}$ PMs; in particular, results for 3- and 4-$\mathcal{UU}$ PMs are presented. Finally, Sec. 4 presents a simple yet effective way of generating additional constraints for avoiding passive constraint singularities, namely by applying an angle-equalizing device on the inner revolute joints of each $\mathcal{UU}$ leg.

2 Constraint and Singularity Analysis of N-$\mathcal{UU}$ PMs

In reference to C1) and C2) in Sec. 1, the most general N-$\mathcal{UU}$ PMs may have a geometry as illustrated in Fig. 1(c). Without loss of generality, we assume that the mechanism has N-fold axial symmetry about the **z**-axis (the fixed reference frame **o-xyz** is shown in Fig. 1, with **xy** being the symmetry plane in the home configuration). The direction vectors of the revolute joints in leg i will be denoted as $\mathbf{w}_{i1}^+, \mathbf{w}_{i2}^+, \mathbf{w}_{i2}^-$ and $\mathbf{w}_{i1}^-$, and their joint angles will be correspondingly denoted as $\theta_{i1}^+, \theta_{i2}^+, \theta_{i2}^-$ and θ_{i1}^-. Due to mirror symmetry, the two pairs $(\mathbf{w}_{i1}^+, \mathbf{w}_{i1}^-)$ and $(\mathbf{w}_{i2}^+, \mathbf{w}_{i2}^-)$ intersect on the symmetry plane at $\mathbf{s}_{i1}$ and $\mathbf{s}_{i2}$, respectively. As long as only rotational motion is concerned, a total of three angular parameters, namely α, β and γ, are needed to specify the kinematics of the mechanism.

It was proved in [15] that the N-$\mathcal{UU}$ PM is a zero-torsion mechanism [3], so that its rotation matrix has the form $e^{2\psi\widehat{\mathbf{w}}}$, where $\mathbf{w} = \mathbf{x}\cos\phi + \mathbf{y}\sin\phi, \phi \in [0, 2\pi], \psi \in [0, \pi/2]$ and $\widehat{\mathbf{w}}$ is a 3×3 skew-symmetric matrix satisfying $\widehat{\mathbf{w}}\mathbf{v} = \mathbf{w} \times \mathbf{v}, \forall \mathbf{v} \in \mathbb{R}^3$. We refer to $e^{2\psi\widehat{\mathbf{w}}}$ as the *tilt motion* about the *tilt axis* **w**, with the *tilt angle* being 2ψ. By utilizing symmetric space theory [16], we characterized the geometric properties of the N-$\mathcal{UU}$ motion in [14], as follows. The symmetric chain $(\mathbf{w}_{i1}^+, \mathbf{w}_{i2}^+, \mathbf{w}_{i2}^-, \mathbf{w}_{i1}^-)$ generates the tilt motion under the symmetric movement condition

$$\theta_{ij}^+ = \theta_{ij}^- = \theta_{ij},\ i = 1, \ldots, \mathrm{N},\ j = 1, 2 \tag{1}$$

i.e., for any tilt axis $\mathbf{w} = \mathbf{x}c_\phi + \mathbf{y}s_\phi,\ \phi \in [0, 2\pi]$ and half-tilt angle ψ (within a singularity-free workspace), there is a unique pair $(\theta_{11}, \theta_{12}) \in [0, 2\pi]^2$ such that

$$e^{\theta_{i1}\widehat{\mathbf{w}}_{i1}^+} e^{\theta_{i2}\widehat{\mathbf{w}}_{i2}^+} e^{\theta_{i2}\widehat{\mathbf{w}}_{i2}^-} e^{\theta_{i1}\widehat{\mathbf{w}}_{i1}^-} = e^{2\psi\widehat{\mathbf{w}}} \tag{2}$$

The symmetry plane passes through $\underline{\mathbf{o}}$, the instantaneous location of **o**, and is perpendicular to $e^{\psi\widehat{\mathbf{w}}}\mathbf{z}$ at a generic configuration $e^{2\psi\widehat{\mathbf{w}}}$. The distal center $\mathbf{s}^-$ rotates about the fixed proximal center $\mathbf{s}^+$, with unit direction **w** of the end-effector, but with a magnitude ψ being half that of the end-effector; $\underline{\mathbf{o}}$ remains the center of the line segment $\mathbf{s}^- - \mathbf{s}^+ = e^{\psi\widehat{\mathbf{w}}}(2d\mathbf{z})$ (with a fixed length of $2d$) under full-cycle motion (see Fig. 2(a)).

Each $\mathcal{UU}$ leg contributes to a 2-D constraint wrench system spanned by two zero-pitch wrenches, with one (denoted $\boldsymbol{\zeta}_{i1}$) passing through $\mathbf{s}_{i1}$ and $\mathbf{s}_{i2}$ and the other (denoted $\boldsymbol{\zeta}_2$) passing through $\mathbf{s}^+$ and $\mathbf{s}^-$; $\boldsymbol{\zeta}_2$ is identical for all legs [4]. The constraint wrenches are denoted by blue arrows in Fig. 2(b). When choosing $\mathbf{w}_{11}^+$ and $\mathbf{w}_{21}^+$ as the actuation joints, the actuation wrenches $\boldsymbol{\zeta}_{a1}$ and $\boldsymbol{\zeta}_{a2}$ may be chosen as the zero-pitch wrenches lying on $\mathbf{s}_{12}\mathbf{s}^-$ and $\mathbf{s}_{22}\mathbf{s}^-$ respectively, as illustrated by the red arrows in Fig. 2. For convenience, we shall denote the unit force vector of a constraint wrench $\boldsymbol{\zeta}_{(\cdot)}$ by $\mathbf{f}_{(\cdot)}$. More details can be found in [14].

Using the aforementioned notation for active and passive constraint wrenches, we can formulate the *static singularity* (leading to a loss of control of the PM, [5]) of a N-$\mathcal{UU}$ PM as

$$\sigma_1\left(\boldsymbol{\zeta}_{11}\ \boldsymbol{\zeta}_{21}\ \ldots\ \boldsymbol{\zeta}_{\mathrm{N}1}\ \boldsymbol{\zeta}_2\ \boldsymbol{\zeta}_{a1}\ \boldsymbol{\zeta}_{a2}\right) = 0 \tag{3}$$

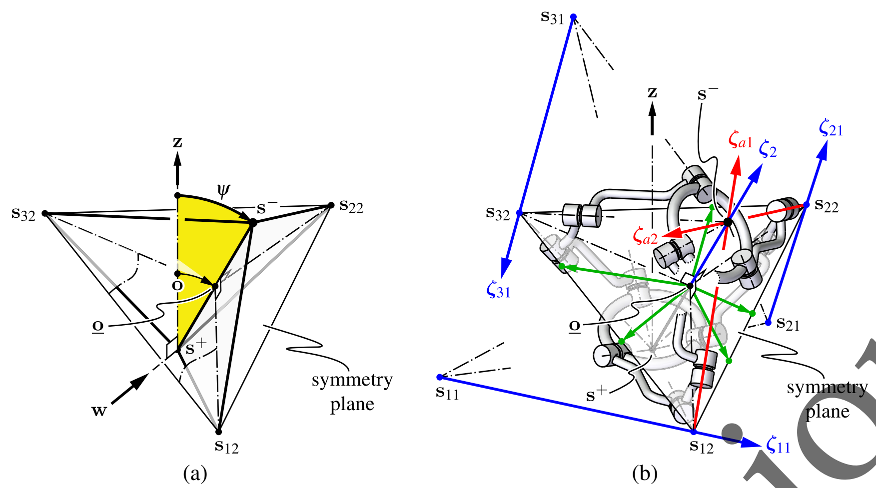

Fig. 2 (a) displacement kinematics of the 3-$\mathcal{UU}$ PM; (b) twists (green), constraint wrenches (blue) and actuation wrenches (red) of the 3-$\mathcal{UU}$ PM.

where σ_1 denotes the smallest singular value of a matrix. Since all constraint and actuation wrenches have zero pitch, we can readily apply the Grassmann-Cayley Algebra (GCA) techniques [1, 9] to further decompose the static singularity. It is proved in [14] that the static singularity may be decomposed into an *active constraint singularity* (ACS) characterized by:

$$\sigma_1\left(\mathbf{f}_2\ \mathbf{f}_{a1}\ \mathbf{f}_{a2}\right) = 0 \tag{4}$$

and a *passive constraint singularity* (PCS) characterized by:

$$\sigma_1\left(\boldsymbol{\tau}_{11}\ \boldsymbol{\tau}_{21}\ \dots\ \boldsymbol{\tau}_{\mathrm{N}1}\right) = 0 \tag{5}$$

where $\boldsymbol{\tau}_{i1}$ is the normalized torque (about $\mathbf{s}^-$) generated by $\boldsymbol{\zeta}_{i1}$, and therefore is given by $\mathbf{w}_{i1}^- \times \mathbf{w}_{i2}^- / \|\mathbf{w}_{i1}^- \times \mathbf{w}_{i2}^-\|$.

3 Optimal Design of General Geometry N-$\mathcal{UU}$ PMs

As shown in Sec. 2, ACS and PCS may be characterized by the rank degeneracy of a bundle of forces and a bundle of torques, respectively. Geometrically, this corresponds to the force or torque bundles degenerating to a pencil. In the former case, there exists a vector $\mathbf{v} \in \mathbb{R}^3$ (perpendicular to the pencil) such that

$$\mathbf{v}^T \mathbf{f}_{a1} = \mathbf{v}^T \mathbf{f}_{a2} = \mathbf{v}^T \mathbf{f}_2 = 0 \tag{6}$$

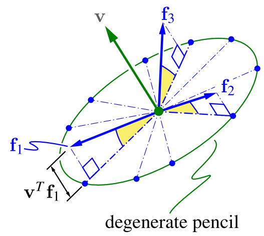

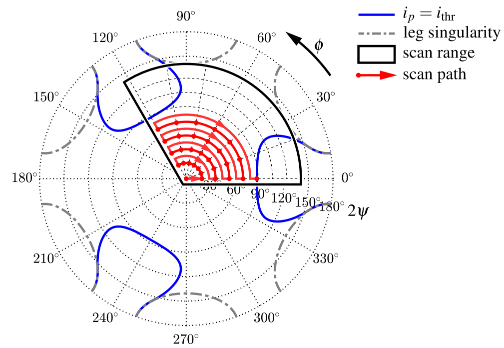

Fig. 3 (a) Least square approximation of a subbundle of unit vectors $\mathbf{f}_i$'s to a degenerate pencil with normal $\mathbf{v}$; (b) sequential scan over the workspace of a 3-$\mathcal{UU}$ PM for maximal PCS-free tilt angle.

The closeness to an ACS may then be measured by the following index:

$$\begin{aligned} i_a \triangleq \sigma_1\left(\mathbf{f}_{a1}\ \mathbf{f}_{a2}\ \sqrt{\mathrm{N}}\mathbf{f}_2\right) &= \min_{\|\mathbf{v}\|=1}\left(\mathbf{v}^T\left(\mathbf{f}_{a1}\mathbf{f}_{a1}^T+\mathbf{f}_{a2}\mathbf{f}_{a2}^T+\sum_{i=1}^{\mathrm{N}}\mathbf{f}_2\mathbf{f}_2^T\right)\mathbf{v}\right)^{1/2} \\ &= \min_{\|\mathbf{v}\|=1}\left((\mathbf{v}^T\mathbf{f}_{a1})^2+(\mathbf{v}^T\mathbf{f}_{a2})^2+\sum_{i=1}^{\mathrm{N}}(\mathbf{v}^T\mathbf{f}_2)^2\right)^{1/2} \end{aligned} \tag{7}$$

which equals the minimum value, over all possible choices of $\mathbf{v}$, of the root sum square of the projected length of $\mathbf{f}_{a1}$, $\mathbf{f}_{a2}$ and (N copies of) $\mathbf{f}_2$ onto $\mathbf{v}$ (see Fig. 3(a)) [13]. Similarly, the PCS measure, denoted as i_p, can be defined as:

$$i_p \triangleq \sigma_1\left(\boldsymbol{\tau}_{11}\ \boldsymbol{\tau}_{21}\ \cdots \boldsymbol{\tau}_{\mathrm{N}1}\right) = \min_{\|\mathbf{w}\|=1}\left(\mathbf{w}^T\left(\sum_{i=1}^{\mathrm{N}}\boldsymbol{\tau}_{i1}\boldsymbol{\tau}_{i1}^T\right)\mathbf{w}\right)^{1/2} \tag{8}$$

The advantage of adopting the above singularity measures is two-fold. First, their definition is independent of the number of $\mathcal{UU}$ legs in the PM. Second, since only pure forces or pure torques are involved, it is obviously frame and scale independent.

The optimal design may be formulated as follows:

O1) **Maximization of the tilt angle subject to a singularity margin constraint:**

$$\max_{(\alpha,\beta,\gamma)} \quad 2\psi_S \tag{9}$$

where

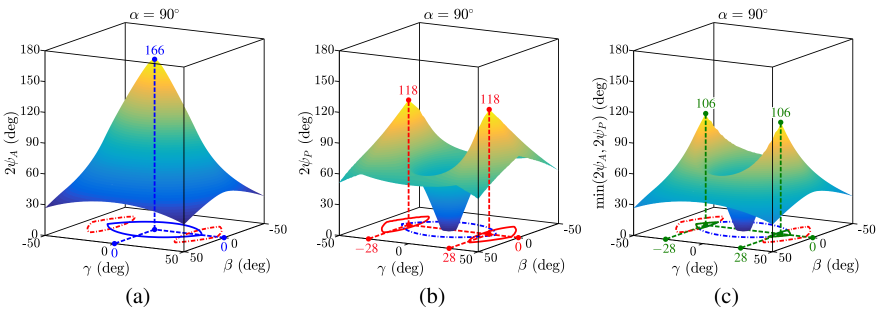

Fig. 4 Distribution of maximal tilt angle of a 3-$\mathcal{UU}$ PM over $(\beta,\gamma) \in [-50°, 50°]^2$ with α fixed at 90° and $i_{\text{thr}} = 0.1$. (a) $2\psi_A$; (b) $2\psi_P$; (c) $2\psi_S$.

$$\begin{aligned} 2\psi_A &= \max\{2\psi \mid i_A(\phi,\psi) \geq i_{\text{thr}},\ \forall\phi \in [0,2\pi]\} \\ 2\psi_P &= \max\{2\psi \mid i_P(\phi,\psi) \geq i_{\text{thr}},\ \forall\phi \in [0,2\pi]\} \\ 2\psi_S &= \min\{2\psi_A, 2\psi_P\} \end{aligned} \tag{10}$$

Once a singularity margin i_{thr} is designated, we may proceed with O1) as follows. First, we set the parameter space $\{(\alpha,\beta,\gamma)\}$ to a bounded cube $[\alpha_{\min},\alpha_{\max}] \times [\beta_{\min},\beta_{\max}] \times [\gamma_{\min},\gamma_{\max}]$, and discretize it to a reasonably fine grid. Next, for a particular point (α,β,γ) on the grid, we may sequentially scan a grid of configurations (ϕ,ψ) for a minimal tilt angle 2ψ that violates the ACS or PCS margin i_{thr} for a certain ϕ. This value corresponds exactly to $2\psi_A$ or $2\psi_P$. To accelerate the scan process, we utilize the N-fold symmetry of the PCS (resulting from that of the N-$\mathcal{UU}$ PM) by restricting ϕ to $[0, 2\pi/\text{N}]$ (see Fig. 3(b)). The distribution of $2\psi_A, 2\psi_P$ and $2\psi_S$ versus $(\beta,\gamma) \in [-50°, 50°]^2$, $\alpha = 90°$ are illustrated in Fig. 4 for the case $\text{N} = 3$. Note from the $\mathcal{UU}$ leg geometry that (α,β,γ), $(\alpha,-\beta,-\gamma)$, $(\pi-\alpha,\beta,-\gamma)$ and $(\pi-\alpha,-\beta,\gamma)$ all lead to the same singularity behavior (as can be observed in Fig. 4). To resolve such redundancy, we shall hereafter narrow down the parameter space to $\alpha \in [45°, 90°]$, $\beta \in [-45°, 45°]$ and $\gamma \in [0, 45°]$. It may be inferred from Fig. 4(a) that a larger ACS-free tilt angle is achieved with β and γ taking values closer to zero. However, such parameter values lead to a very low PCS-free tilt angle (Fig. 4(b)). A compromise is acthieve with β remaining close to and γ substantially deviating from zero (Fig. 4(c)).

We emphasize that an optimal design for N-$\mathcal{UU}$ PMs following O1) should be based on a physically meaningful (see [13] for some discussion) singularity margin value i_{thr}, which are usually not available at conceptual design stage [2, Ch. 6]. Alternatively, we may seek to maximize the minimal singularity measure over a fixed prescribed workspace (e.g. $2\psi \in [0, \pi/2]$):

Table 1 Optimal design results of 3- and 4-$\mathcal{UU}$ PMs for formulation O2).

number of legs	angle-eq. device	max i_{thr}	α	β	γ
3	No	0.210	90	0	29
	Yes	0.454	90	0	14
4	No	0.521	82	12	20
	Yes	0.637	88	−2	13

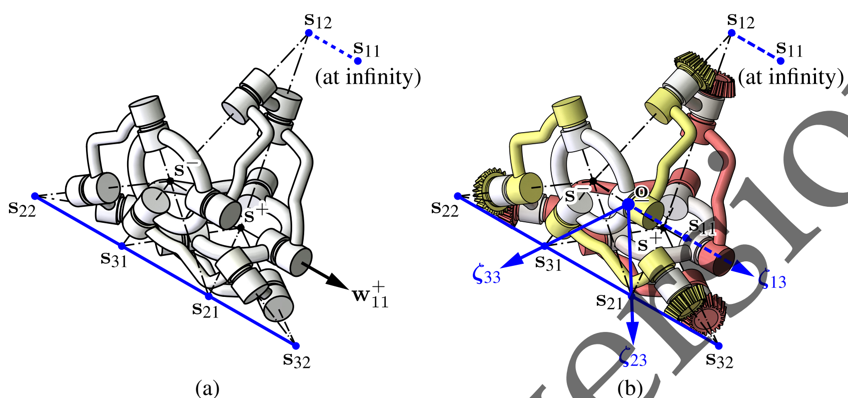

Fig. 5 (a) A configuration of PCS for a 3-$\mathcal{UU}$ PM ($\alpha = 90°$, $\beta = 0°$, $\gamma = 20°$); (b) avoidance of the PCS configuration by imposing angle-equalizing devices.

O2) **Maximization of the minimal singularity measure over a prescribed workspace:**

$$\max_{(\alpha,\beta,\gamma)} \quad i_{\text{thr}}$$
$$\text{s.t.} \begin{cases} i_{\text{thr}} \le \min\limits_{(\phi,\psi)} \; i_A(\phi,\psi) \\ i_{\text{thr}} \le \min\limits_{(\phi,\psi)} \; i_P(\phi,\psi) \end{cases} \quad \begin{cases} 0 \le \phi \le 2\pi \\ 0 \le 2\psi \le \pi/2 \end{cases} \tag{11}$$

O2) can be solved with an approach similar to that of O1). The optimal margin value and corresponding parameters for 3- and 4-$\mathcal{UU}$ PMs are given in Tab. 1.

4 Angle-Equalizing Device

According to the symmetric movement condition Eq. (1), each revolute joints pair $(\mathbf{w}_{ij}^+, \mathbf{w}_{ij}^-)$ is instantaneously equivalent to a single revolute joint along $\mathbf{w}_{ij}^+ + \mathbf{w}_{ij}^-$ (see Fig. 1(d)). However, as the symmetric movement condition is enforced by the loop-closure constraint of the N-$\mathcal{UU}$ PM, such equivalence does not hold in constraint analysis.

Motivated by the above observation, we consider imposing an angle-equalizing device onto the inner revolute pair $(\mathbf{w}_{i2}^{+}, \mathbf{w}_{i2}^{-})$ of each leg i, via for example a bevel gear pair. This does turn each $\mathcal{UU}$ leg into a 3-DoF leg that is instantaneously equivalent to a $\mathcal{RRR}$ leg with unit direction vectors $(\mathbf{w}_{i1}^{+}, \mathbf{w}_{i2}, \mathbf{w}_{i1}^{-})$, $\mathbf{w}_{i2} = (\mathbf{w}_{i2}^{+} + \mathbf{w}_{i2}^{-})/\|\mathbf{w}_{i2}^{+} + \mathbf{w}_{i2}^{-}\|$. It is easy to verify for each $\mathcal{UU}$ leg that an additional constraint wrench, denoted as $\boldsymbol{\zeta}_{i3}$, emerges, and it can be identified as the zero-pitch wrench along $\underline{\mathbf{o}}\mathbf{s}_{i1}$. Since $\boldsymbol{\zeta}_{i3},\ i = 1,\ldots,\mathrm{N}$ all lie in the symmetry plane, they help to avoid PCSs. Figure 5(a) illustrates a 3-$\mathcal{UU}$ PM at a configuration of PCS. In this particular case, $\mathbf{s}_{21}$, $\mathbf{s}_{22}$, $\mathbf{s}_{31}$ and $\mathbf{s}_{32}$ become collinear and therefore $\boldsymbol{\zeta}_{21}$ and $\boldsymbol{\zeta}_{31}$ become linearly dependent. With the imposition of an angle-equalizing devices on the PM, as illustrated in Fig. 5(b), the PCS is avoided with the presence of three extra passive constraint wrenches $\boldsymbol{\zeta}_{13}, \boldsymbol{\zeta}_{23}$ and $\boldsymbol{\zeta}_{33}$. Consequently, the definition for the PCS measure given in Eq. (8) may be changed to:

$$
\begin{aligned}
i_p &\triangleq \sigma_1 \left(\boldsymbol{\tau}_{11}\ \boldsymbol{\tau}_{13}\ \boldsymbol{\tau}_{21}\ \boldsymbol{\tau}_{23}\ \ldots \boldsymbol{\tau}_{\mathrm{N}1}\ \boldsymbol{\tau}_{\mathrm{N}3} \right) \\
&= \min_{\|\mathbf{w}\|=1} \left(\mathbf{w}^T \left(\sum_{i=1}^{\mathrm{N}} \left(\boldsymbol{\tau}_{i1}\boldsymbol{\tau}_{i1}^T + \boldsymbol{\tau}_{i3}\boldsymbol{\tau}_{i3}^T \right) \right) \mathbf{w} \right)^{1/2}
\end{aligned}
\tag{8'}
$$

where $\boldsymbol{\tau}_{i3}$ is a normalized torque (about $\mathbf{s}^{-}$) generated by $\boldsymbol{\zeta}_{i3}$, and is given by $(\mathbf{s}_{i1} - \underline{\mathbf{o}}) \times (\mathbf{s}^{-} - \underline{\mathbf{o}})/\|(\mathbf{s}_{i1} - \underline{\mathbf{o}}) \times (\mathbf{s}^{-} - \underline{\mathbf{o}})\|$. The optimal design results, for O2), of 3- and 4-$\mathcal{UU}$ PMs with angle-equalizing devices are also presented in Tab. 1. The 4-$\mathcal{UU}$ PM with or without angle-equalizing device has higher singularity margin than its three-legged counterpart. Second, since the angle-equalizing device helps to avoid PCSs, γ is allowed to take a smaller value to increase the ACS margin (Cf. the discussion about Fig. 4).

5 Conclusions

We conclude our paper with two remarks. First, the optimal parameter values of general-geometry N-$\mathcal{UU}$ PMs listed in Tab. 1, to some extent, agree with those acquired with a special geometry ($\alpha = 90°, \beta = 0°$; see [14]). Second, the actual workspace of N-$\mathcal{UU}$ PMs is also limited by potential link collisions. In practice, this issue may be solved by iterative design/collision checking in CAD modeling software. Otherwise, a systematic solution may be derived by following the approach proposed in [7].

Acknowledgements The authors gratefully acknowledge the financial support of the Italian Ministry of Education, Universities and Research through the PRIN Grant no. 20124SMZ88. This work is also in partial fulfillment to China National Natural Science Foundation Grant no. 51375413, which supported Dr. Wu when he was working at HKUST.

References

1. Ben-Horin, P., Shoham, M.: Application of Grassmann–Cayley algebra to geometrical interpretation of parallel robot singularities. The International Journal of Robotics Research **28**(1), 127–141 (2009)
2. Bohigas, O.: Numerical computation and avoidance of manipulator singularities. Ph.D. thesis, Universidad Politécnica de Cataluña (2013)
3. Bonev, I., Zlatanov, D., Gosselin, C.: Advantages of the modified Euler angles in the design and control of PKMs. In: 2002 Parallel Kinematic Machines International Conference, pp. 171–188. Citeseer (2002)
4. Carricato, M.: Decoupled and homokinetic transmission of rotational motion via constant-velocity joints in closed-chain orientational manipulators. Journal of Mechanisms and Robotics **1**(4), 041,008 (2009)
5. Conconi, M., Carricato, M.: A new assessment of singularities of parallel kinematic chains. IEEE Transactions on Robotics **25**(4), 757–770 (2009)
6. Culver, I.H.: Constant velocity universal joint (1969). US Patent 3,477,249
7. Gosselin, C.M., Hamel, J.F.: The agile eye: a high-performance three-degree-of-freedom camera-orienting device. In: Robotics and Automation, 1994. Proceedings., 1994 IEEE International Conference on, pp. 781–786. IEEE (1994)
8. Hunt, K.: Constant-velocity shaft couplings: a general theory. Journal of Engineering for Industry **95**(2), 455–464 (1973)
9. Kanaan, D., Wenger, P., Caro, S., Chablat, D.: Singularity analysis of lower mobility parallel manipulators using Grassmann–Cayley algebra. IEEE Transactions on Robotics **25**(5), 995–1004 (2009)
10. Kong, X., Yu, J., Li, D.: Reconfiguration analysis of a two degrees-of-freedom 3-4R parallel manipulator with planar base and platform. Journal of Mechanisms and Robotics **8**(1), 011,019 (2016)
11. Rosheim, M.E., Sauter, G.F.: New high-angulation omni-directional sensor mount. In: International Symposium on Optical Science and Technology, pp. 163–174. International Society for Optics and Photonics (2002)
12. Sone, K., Isobe, H., Yamada, K.: High angle active link. Special Issue Special Supplement to Industrial Machines (2004)
13. Voglewede, P.A., Ebert-Uphoff, I.: Overarching framework for measuring closeness to singularities of parallel manipulators. IEEE Transactions on Robotics **21**(6), 1037–1045 (2005)
14. Wu, Y., Carricato, M.: Synthesis and singularity analysis of n-$\mathcal{UU}$ parallel wrists: a symmetric subspace approach. In: International Design Engineering Technical Conferences & Computers and Information in Engineering Conference. American Society of Mechanical Engineers (2017). Submitted
15. Wu, Y., Li, Z., Shi, J.: Geometric properties of zero-torsion parallel kinematics machines. In: Intelligent Robots and Systems (IROS), 2010 IEEE/RSJ International Conference on, pp. 2307–2312. IEEE (2010)
16. Wu, Y., Löwe, H., Carricato, M., Li, Z.: Inversion symmetry of the Euclidean group: Theory and application to robot kinematics. IEEE Transactions on Robotics **32**(2), 312–326 (2016)